Macromolecules

pubs.acs.org/Macromolecules Article

Coexistence of Polymeric Microemulsion with Homopolymer-Rich Phases

Russell K. W. Spencer* and Mark W. Matsen*

Cite This: *Macromolecules* 2021, 54, 1329−1337 Read Online

ACCESS | Metrics & More | Article Recommendations | Supporting Information

ABSTRACT: Recent field-theoretic simulations of symmetric ternary blends of A- and B-type homopolymers with AB diblock copolymer [Vorselaars, B.; et al. *Phys. Rev. Lett.*, **2020**, *125*, 117801]predicted three-phase coexistence between bicontinuous microemulsion (BμE) and two homopolymer-rich phases. The present study begins by repeating their grand-canonical simulations over longer durations in simulation boxes of different sizes to ensure that the prediction was not an artifact of nonequilibrium effects or finite system sizes. The coexistence is then demonstrated in canonical simulations, where the three phases are explicitly separated by interfaces. From those simulations, we extract the interfacial widths, the interfacial tensions, the domain size in the BμE phase, and the copolymer concentration in each phase. The latter results are used to improve the accuracy of the previous phase diagram.

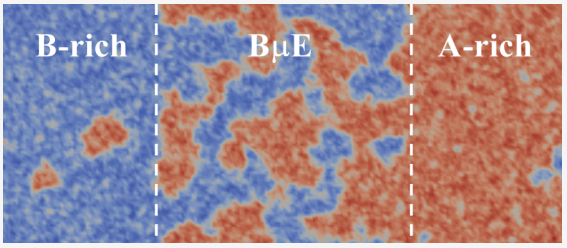

INTRODUCTION

Bicontinuous microemulsion (BμE) is a well-established phase of lyotropic liquid crystals, where oil and water mix together on the nanoscale forming interweaving domains separated by a monolayer of surfactant molecules.[1,2] It is known for its use in enhanced oil recovery[3] but also has numerous other applications.[2] In 1997, Bates et al.[4] discovered an equivalent polymeric BμE in ternary blends of incompatible polyethylene (PE) and poly(ethylenepropylene) (PEP) homopolymers, where PE−PEP diblock copolymers serve as the surfactant. BμE has since been observed in other polymeric systems[5−13] and is being studied for a variety of applications including stable polymeric alloys,[14] nanoporous functional materials,[15] solar cells,[16,17] fuel cells,[18] and rechargeable batteries.[18,19]

The behavior observed by the experiments, which are generally conducted for homopolymer-to-copolymer size ratios of $\alpha = N_h/N_c = 0.2$, is depicted in the schematic phase diagram of Figure 1a, which is plotted in terms of temperature, T, and copolymer volume fraction, $\bar{\phi}_c$. Without copolymer ($\bar{\phi}_c = 0$), the two homopolymers macrophase-separate into coexisting (A + B) phases as T is reduced, while neat symmetric diblock copolymer melts ($\bar{\phi}_c = 1$) microphase-separate into an ordered lamellar (LAM) phase. Between these two regions, researchers observe a narrow channel of BμE extending toward $T = 0$. Note that the BμE is a part of the disordered (DIS) phase, where the A- and B-rich domains are well segregated but lack the long-range order of the LAM phase.

This experimental behavior is in stark contrast to the predictions of self-consistent field theory (SCFT), which is generally one of the most successful theories in soft condensed matter.[20] For this system, however, SCFT fails to predict BμE, instead predicting the A + B and LAM regions to be separated by

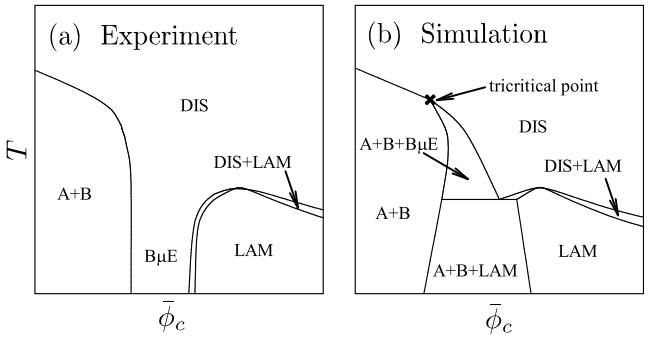

Figure 1. Schematic (a) experimental and (b) field-theoretic simulation (FTS) phase diagrams plotted in terms of copolymer volume fraction, $\bar{\phi}_c$, and temperature, T. The labels A, B, LAM, DIS, and BμE denote A-homopolymer-rich, B-homopolymer-rich, lamellar, disordered, and bicontinuous microemulsion, respectively.

A + B + LAM coexistence,[21−23] which terminates in a Lifshitz critical point at high temperature.[24] The difference between experiment and SCFT is attributed to fluctuation effects,[25,26] which are controlled by the invariant polymerization index of, for example, the homopolymers, $\bar{N}_h = a^6\rho_0^2 N_h$, where a is the average segment length and ρ_0 is the bulk segment density. Although the experimental phase diagram differs substantially, it

Received: December 1, 2020
Revised: January 11, 2021
Published: January 25, 2021

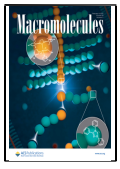

https://dx.doi.org/10.1021/acs.macromol.0c02668
Macromolecules 2021, 54, 1329−1337

should nevertheless evolve continuously to the SCFT phase diagram as $\bar{N}_h$ diverges to infinity. Furthermore, the Lifshitz point cannot appear prior to this limit,[27] as required by our understanding that its lower critical dimension is 4.[28−31] It is hard to fathom how this is possible.

Recent field-theoretic simulations (FTS)[32] have proposed the alternative phase diagram in Figure 1b, which is free of this inconsistency. Instead of the BμE channel, it exhibits A + B + LAM coexistence at low temperature and A + B + BμE coexistence at high temperature, which eventually terminates at a tricritical point. The convergence to the SCFT diagram, as $\bar{N}_h \to \infty$, is achieved by shrinking the A + B + BμE region into a Lifshitz point, while all of the other FTS phase boundaries shift continuously toward their SCFT counterparts. Interestingly, simulations of the bond-fluctuation model[33] predicted the same topology prior to the experiments, albeit for much different parameter values of $\alpha = 1$ and $\bar{N}_h = 145$. Furthermore, this phase behavior is more consistent with lyotropic liquid crystals, where the microemulsions commonly coexist with water- and oil-rich phases.[1−3]

The three-phase coexistence in SCFT and FTS can be attributed to an attraction between the diblock monolayers of the lamellar and microemulsion phases, which limits the size of their domains. However, the attraction is extraordinarily weak,[23,34] which could explain why coexistence was not observed in the experiments. The experiments were performed by equilibrating samples of the DIS phase at a given $\bar{\phi}_c$ and then looking for a transition as T was slowly decreased. When the system encounters the three-phase region, the BμE should expel excess homopolymer into A- and B-rich domains. This would occur by nucleation and growth, which is naturally a slow process but even more so given the unusually small energy gain. The energy gain would have been further limited by the fact that the experiments did not generally probe a significant distance into the supposed BμE channel. Thus, the time scale of the experiments may simply have been too short for nucleation to occur. Not always though, Xie et al.[19] recently reported evidence of macrophase separation.

Here, the A + B + BμE coexistence region is examined in greater detail. The study begins with a finite-size analysis of the previous grand-canonical simulations[32] to ensure that their prediction of coexistence was not an artifact of small simulation boxes. Once that is established, the coexistence is examined in the canonical ensemble, where the three phases are separated by explicit interfaces. From these latter simulations, we extract interfacial properties, details of the coexisting phases, and accurate phase boundaries.

FIELD-THEORETIC SIMULATIONS

The FTS in this study are performed for incompressible blends of n_{hA} A-type homopolymers, n_{hB} B-type homopolymers, and n_c AB diblock copolymers. They focus on symmetric conditions where both homopolymers have N_h segments and both blocks of the copolymer have $N_c/2$ segments. Here, segments are defined based on a common volume of ρ_0^{-1}, such that the total volume of the system is $V = N_h(n_{hA} + n_{hB} + n_c/\alpha)/\rho_0$, where $\alpha = N_h/N_c$. As part of the symmetry, the statistical lengths of the A and B segments are both set to a. Thus, the two homopolymers have the same unperturbed end-to-end length, $R_h = a\sqrt{N_h}$, which is used as our unit of length. To assess how the components of the blend segregate, we define the composition profile

$$\hat{\phi}_-(\mathbf{r}) = \hat{\phi}_{hA}(\mathbf{r}) + \hat{\phi}_{cA}(\mathbf{r}) - \hat{\phi}_{hB}(\mathbf{r}) - \hat{\phi}_{cB}(\mathbf{r}) \tag{1}$$

expressed in terms of A and B contributions from the homopolymers (h) and copolymers (c). We also define the total segment profile

$$\hat{\phi}_+(\mathbf{r}) = \hat{\phi}_{hA}(\mathbf{r}) + \hat{\phi}_{cA}(\mathbf{r}) + \hat{\phi}_{hB}(\mathbf{r}) + \hat{\phi}_{cB}(\mathbf{r}) \tag{2}$$

which is constrained to one so as to enforce incompressibility. The last quantity of interest is the copolymer concentration profile

$$\hat{\phi}_c(\mathbf{r}) = \hat{\phi}_{cA}(\mathbf{r}) + \hat{\phi}_{cB}(\mathbf{r}) \tag{3}$$

From these profiles, the blend composition is given by

$$\bar{\phi}_- \equiv \frac{1}{V}\int \hat{\phi}_-(\mathbf{r})\mathrm{d}\mathbf{r} = \frac{(n_{hA} - n_{hB})N_h}{\rho_0 V} \tag{4}$$

and the copolymer content is

$$\bar{\phi}_c \equiv \frac{1}{V}\int \hat{\phi}_c(\mathbf{r})\mathrm{d}\mathbf{r} = \frac{n_c N_c}{\rho_0 V} \tag{5}$$

In polymer field theory,[20,35,36] the partition function of a particle-based Hamiltonian is modified by inserting an expression for the interaction energy involving a composition field, $W_-(\mathbf{r})$, that couples to $\hat{\phi}_-(\mathbf{r})$. Similarly, the Dirac delta functional enforcing incompressibility is replaced by an expression involving a pressure field, $W_+(\mathbf{r})$, that couples to $\hat{\phi}_+(\mathbf{r})$. The introduction of these two identities allows the polymer coordinates to be integrated out, resulting in a field-based Hamiltonian, $H[W_-, W_+]$, of the form

$$\frac{N_h H}{k_B T \rho_0} = \frac{N_h H_Q}{k_B T \rho_0} + \int\left(\frac{W_-^2}{\chi_b N_h} - W_+\right)\mathrm{d}\mathbf{r} \tag{6}$$

where $H_Q[W_-,W_+]$ is the Hamiltonian for an equivalent system of noninteracting polymers acted upon by the fields and χ_b is the bare Flory−Huggins interaction parameter. The first part of our study applies the grand-canonical ensemble with equal homopolymer chemical potentials, for which

$$\frac{N_h H_Q}{k_B T \rho_0} = -Q_{hA} - Q_{hB} - zQ_c \tag{7}$$

where the fugacity, $z = \exp(\mu/k_B T)$, depends on the copolymer chemical potential, μ, relative to that of the homopolymers. The second part of the study employs the canonical ensemble with $\bar{\phi}_- = 0$, for which

$$\frac{N_h H_Q}{k_B T \rho_0 V} = -\frac{1-\bar{\phi}_c}{2}\ln(Q_{hA}) - \frac{1-\bar{\phi}_c}{2}\ln(Q_{hB}) - \alpha\bar{\phi}_c\ln(Q_c) \tag{8}$$

The above expressions involve single-chain partition functions

$$Q_\gamma = \int q_\gamma(\mathbf{r}, s) q_\gamma^\dagger(\mathbf{r}, s)\mathrm{d}\mathbf{r} \tag{9}$$

for the three different molecules (γ = hA, hB, and c). These, in turn, involve partial partition functions, $q_\gamma(\mathbf{r}, s)$ and $q_\gamma^\dagger(\mathbf{r}, s)$, which obey diffusion equations. They are solved in orthorhombic boxes of volume $V = L_x L_y L_z$ with periodic boundary conditions, using a standard pseudo-spectral algorithm with Richardson extrapolation.[37,38] Note that this numerical method

https://dx.doi.org/10.1021/acs.macromol.0c02668
Macromolecules 2021, 54, 1329−1337

defines all spatially dependent quantities at the nodes of a regular $m_x \times m_y \times m_z$ grid, where $L_x = m_x\Delta$, $L_y = m_y\Delta$, and $L_z = m_z\Delta$ are each restricted to an integer number of grid spacings, Δ. See ref 39 for further details.

In SCFT, the free energy of the system is approximated by $F = H[w_-, w_+]$, where $w_-(\mathbf{r})$ and $w_+(\mathbf{r})$ represent the saddle-point of the Hamiltonian. The saddle-point is obtained by solving

$$\Lambda(\mathbf{r}) \equiv \phi_-(\mathbf{r}) + \frac{2}{\chi_b N_h} W_-(\mathbf{r}) = 0 \tag{10}$$

$$\phi_+(\mathbf{r}) - 1 = 0 \tag{11}$$

where $\phi_\gamma(\mathbf{r})$ denotes the ensemble average of $\hat{\phi}_\gamma(\mathbf{r})$ in the system of noninteracting polymers. For the grand-canonical ensemble

$$\phi_{hA}(\mathbf{r}) = \int_0^1 q_{hA}(\mathbf{r}, s) q_{hA}^\dagger(\mathbf{r}, s) \mathrm{d}s \tag{12}$$

$$\phi_{cA}(\mathbf{r}) = z \int_0^{1/2\alpha} q_c(\mathbf{r}, s) q_c^\dagger(\mathbf{r}, s) \mathrm{d}s \tag{13}$$

and for the canonical ensemble

$$\phi_{hA}(\mathbf{r}) = \frac{(1 - \bar{\phi}_c)V}{2Q_{hA}} \int_0^1 q_{hA}(\mathbf{r}, s) q_{hA}^\dagger(\mathbf{r}, s) \mathrm{d}s \tag{14}$$

$$\phi_{cA}(\mathbf{r}) = \frac{\alpha \bar{\phi}_c V}{Q_c} \int_0^{1/2\alpha} q_c(\mathbf{r}, s) q_c^\dagger(\mathbf{r}, s) \mathrm{d}s \tag{15}$$

The expressions for the B components are analogous.

In FTS, one instead simulates the Hamiltonian $H[W_-,W_+]$. Here, however, we reduce the simulations to a single fluctuating field, by applying a partial saddle-point approximation, whereby $W_+(\mathbf{r})$ is replaced by $w_+(\mathbf{r})$. The saddle-point eq 11 for $w_+(\mathbf{r})$ is solved iteratively using Anderson mixing.[40] The remaining field is evolved using the Langevin dynamics

$$W_-(\mathbf{r}; \tau + \delta\tau) = W_-(\mathbf{r}; \tau) - \Lambda(\mathbf{r}; \tau)\delta\tau + \mathcal{N}(0, \sigma) \tag{16}$$

where τ denotes the simulation time. Thermal noise is provided by random numbers from a normal distribution, $\mathcal{N}(0, \sigma)$, of zero mean and $\sigma^2 = 2N_h\delta\tau/\Delta^3\rho_0$ variance. Here, eq 16 is iterated using the predictor−corrector algorithm.[40,41]

Normally, the increments used to represent continuous functions in numerical calculations are chosen small enough that their finite size has no significant effect. However, this is not possible with the grid resolution due to an ultraviolet divergence that occurs as $\Delta \to 0$.[42] Fortunately, for polymers of high molecular weight, this divergence can be removed by expressing results in terms of an effective Flory−Huggins χ parameter defined by[43]

$$\chi = \left(1 - \frac{2.333R_h}{\Delta\sqrt{\bar{N}_h}}\right)\chi_b \tag{17}$$

Our study is performed with $\Delta = 0.75\ R_h$ and $\bar{N}_h = 10^4$, for which the effective interaction parameter is $\chi = 0.969\ \chi_b$.

RESULTS

The previous studies[32,39] identified the A + B + BμE coexistence by monitoring the average copolymer content, $\langle\bar{\phi}_c\rangle$, in grand-canonical simulations as the chemical potential, μ, was changed. This revealed a sudden jump from small $\langle\bar{\phi}_c\rangle$ corresponding to either A- or B-homopolymer-rich configurations to a larger $\langle\bar{\phi}_c\rangle$ corresponding to microemulsion configurations with balanced homopolymer concentrations. However, the microemulsion domains were comparable in size to the simulation boxes, which could potentially cause significant finite-size effects.

We now address this issue by repeating their FTS using cubic simulation boxes of different sizes, $L = 18R_h$, $36R_h$, and $72R_h$. The new results are shown in Figure 2. To ensure they are free of

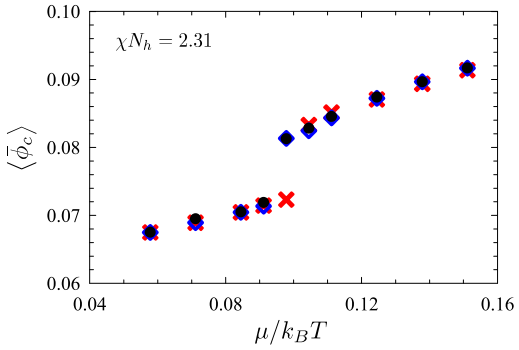

Figure 2. Average copolymer content as a function of chemical potential at $\chi N_h = 2.31$, obtained from grand-canonical FTS using cubic simulation boxes of different sizes, $L/R_h = 18$ (crosses), 36 (diamonds), and 72 (dots).

nonequilibrium effects, two independent simulations are performed for each data point, one initialized with a homopolymer-rich phase and the other with a microemulsion phase obtained from previous simulations at nearby parameter values. The collection of statistics for $\langle\bar{\phi}_c\rangle$ begins only after both have converged to the same phase. Furthermore, Figure 2 includes additional chemical potentials near the jump in $\langle\bar{\phi}_c\rangle$ to help ensure that it is a discontinuous phase transition. For the most part, the different system sizes yield indistinguishable results within the numerical noise. The only exception is at $\mu/k_BT = 0.0978$, where the smallest system exhibits a homopolymer-rich phase, while the two larger systems exhibit the microemulsion phase. Evidently, the limited size of the $L = 18R_h$ box causes a small shift in the transition to higher μ, which in turn increases the copolymer concentrations of the coexisting phases. Nevertheless, the two larger boxes appear free of significant finite-size effects.

To confirm this, we examine fluctuations in the blend composition. Figure 3a plots histograms of $\bar{\phi}_-$ for the homopolymer-rich phase, using each of the three box sizes. As expected, the distributions narrow as the system size increases. Provided the system is sufficiently large, the distributions should become Gaussian with a standard deviation that varies as $\sigma_\phi \propto V^{-1/2}$. Indeed, the distributions are Gaussian to within the obvious statistical noise, and the scaling plot in Figure 3b confirms that σ_ϕ decreases as expected.

Figure 4 repeats the analysis for the microemulsion phase. Again, the smaller system produces a nice Gaussian distribution, centered around zero as required by symmetry. Although the shape deviates significantly from an ideal Gaussian for the two larger systems, the deviations from even symmetry imply that this is just due to limited statistics. In any case, the widths of the distributions conform well with the expected scaling, as demonstrated in Figure 4b. Note that our evaluations of σ_ϕ explicitly assume $\langle\bar{\phi}_-\rangle = 0$.

Now that we have established that our results are free of significant finite-size effects, we perform canonical simulations

https://dx.doi.org/10.1021/acs.macromol.0c02668
Macromolecules 2021, 54, 1329−1337

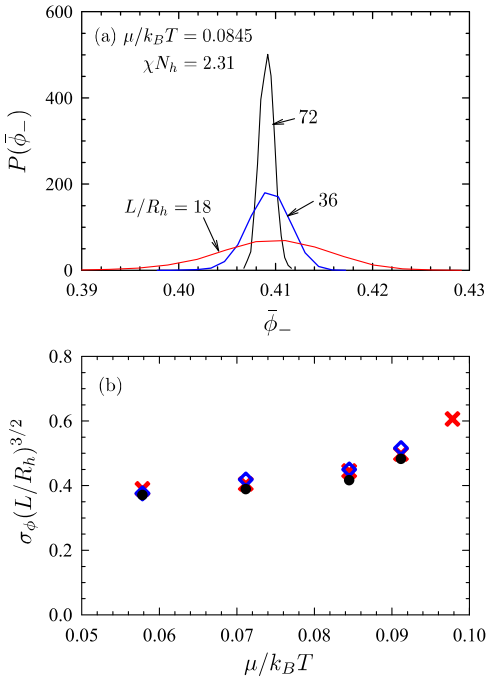

Figure 3. (a) Histogram of the composition calculated for the A-homopolymer-rich phase at μ/k_BT = 0.0845, using different system sizes, L/R_h = 18, 36, and 72. (b) Scaled widths of the distribution as a function of chemical potential for L/R_h = 18 (crosses), 36 (diamonds), and 72 (dots).

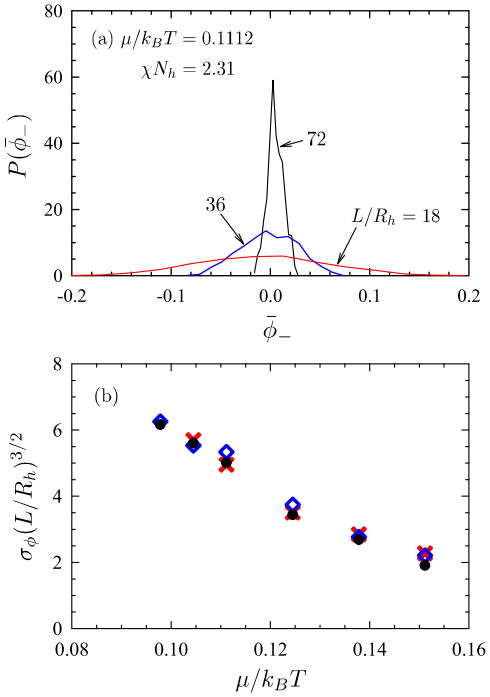

Figure 4. Analogous plots to those of Figure 3 but for the microemulsion phase.

of the three coexisting phases. This is done by taking the individual phases from the largest box of our grand-canonical simulations and splicing them together into one orthorhombic box of size $216R_h \times 72R_h \times 72R_h$. Figure 5 displays equilibrated configurations at three different segregations, χN_h. The microemulsion is in the middle flanked by a B-rich phase to

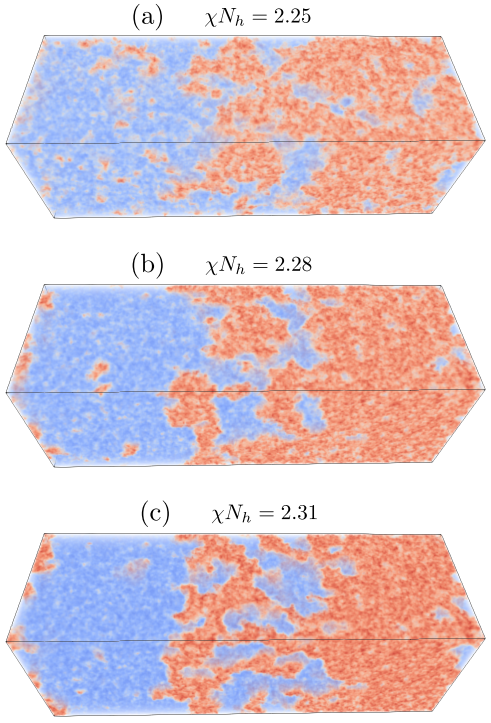

Figure 5. Coexisting B-rich, BμE, and A-rich phases in $216R_h \times 72R_h \times 72R_h$ orthorhombic boxes with periodic boundaries, simulated at different χN_h.

the left and an A-rich phase to the right, creating two interfaces near $x \approx 72R_h$ and $144R_h$. The periodic boundary condition creates a third interface between the two homopolymer-rich phases near $x \approx 0$ (or equivalently $x \approx 216R_h$). The Supporting Information provides a video of the Langevin dynamics for χN_h = 2.31, showing considerable motion of the large microemulsion domains. It illustrates that there is ample time for the volume of each phase to adjust to acquire its preferred copolymer content.

Figure 6 displays the composition, $\langle\phi_-(x)\rangle$, and copolymer, $\langle\phi_c(x)\rangle$, profiles obtained by averaging over the y–z plane. The composition in Figure 6a is reasonably uniform, $\bar{\phi}_-$ = ±0.38, in the homopolymer-rich regions as expected for isotropic phases. Although the composition profile in the microemulsion region is noisy, there is no evidence that the oscillations result from the presence of the interfaces and so it would presumably average to $\bar{\phi}_-$ = 0 over a sufficiently long run. The copolymer profile in Figure 6b is reasonably uniform in all three regions, with $\bar{\phi}_c$ = 0.073 and 0.083 in the homopolymer-rich and microemulsion phases, respectively.

The interfacial widths are plotted in Figure 7 for different values of χN_h. The width of the homopolymer/microemulsion interface, $w_{B\mu E}$, is obtained by fitting the copolymer profile to

$$\langle\phi_c(x)\rangle = c_1 + c_2 \tanh\left(\frac{2(x-x_1)}{w_{B\mu E}}\right) - c_2 \tanh\left(\frac{2(x-x_2)}{w_{B\mu E}}\right) \quad (18)$$

where c_1, c_2, x_1, x_2, and $w_{B\mu E}$ are the fitting parameters. Note that the fit excludes the ends of the box (i.e., $x \approx 0$ and L_x), where the A/B interface exists. Similarly, the width of the A/B interface, w_{AB}, is extracted from an analogous fit to the $\langle\phi_-(x)\rangle$ profile, this time excluding the microemulsion region. It is interesting that $w_{B\mu E}$, which appears somewhat diffuse in Figure 5, is in fact just as narrow as w_{AB}.

https://dx.doi.org/10.1021/acs.macromol.0c02668
Macromolecules 2021, 54, 1329−1337

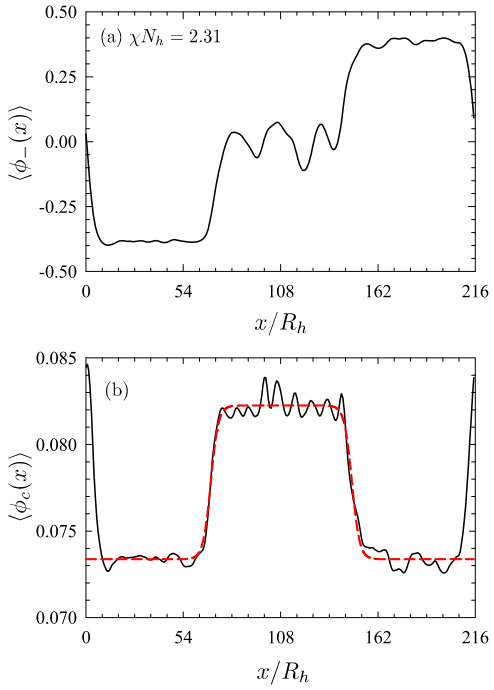

Figure 6. (a) Composition and (b) copolymer concentration profiles for three-phase coexistence at $\chi N_h = 2.31$. The dashed curve in the lower plot denotes a fit to eq 18.

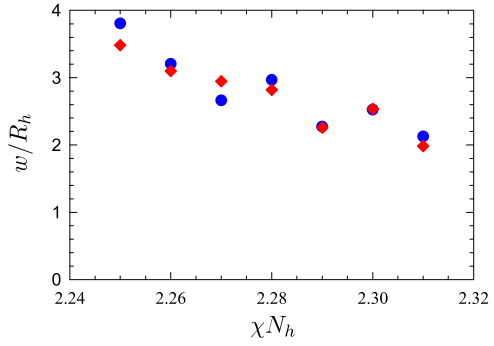

Figure 7. Width of the homopolymer/microemulsion interface, $w_{B\mu E}$ (dots), and the homopolymer/homopolymer interface, w_{AB} (diamonds), in the three-phase coexistence region.

The interfacial tensions are calculated by using the fact that the free energy of the system is $F = F_{bulk} + \gamma_{total} A$, where F_{bulk} is the bulk free energy of the three coexisting phases, γ_{total} is the total tension of the three interfaces, and $A = V/L_x$ is the area of each interface. It thus follows that[39]

$$\gamma_{total} = -\frac{L_x^2}{V}\frac{\partial F}{\partial L_x} = \frac{L_x^2}{V}\left\langle \frac{\partial H_Q}{\partial L_x} \right\rangle \tag{19}$$

where the derivatives are performed at a constant volume (i.e., $L_y = L_z = \sqrt{V/L_x}$). Given that the simulations are performed in the canonical ensemble, we use the H_Q from eq 8. Although there are analytical expressions for the derivatives of Q_γ,[44] we simply evaluate the derivative of H_Q using a finite difference. Because of the periodic boundary condition, γ_{total} has contributions of $\gamma_{B\mu E}$ from each homopolymer/microemulsion interface as well as γ_{AB} from one homopolymer/homopolymer interface. The result, $\gamma_{total} = 2\gamma_{B\mu E} + \gamma_{AB}$, is plotted in Figure 8 with dots. Analogous canonical simulations are also performed

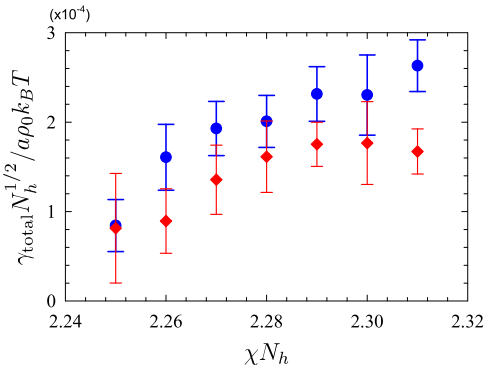

Figure 8. Total interfacial tension for A + B + BμE coexistence, $\gamma_{total} = \gamma_{AB} + 2\gamma_{B\mu E}$ (dots), and for A + B coexistence, $\gamma_{total} = 2\gamma_{AB}$ (diamonds).

for two coexisting homopolymer-rich phases, where the appropriate copolymer content $\bar{\phi}_c$ is determined from the copolymer profile for three-phase coexistence. In this case, the periodic boundary condition results in two homopolymer/homopolymer interfaces. The result, $\gamma_{total} = 2\gamma_{AB}$, is plotted in Figure 8 with diamonds. Not surprisingly, the interfacial tensions are relatively tiny, about 3 orders of magnitude smaller than that of a bare homopolymer/homopolymer interface without any added copolymer.[39] This is the reason for the relatively large error bars, which are estimated from the fluctuations in $\partial H_Q/\partial L_x$.

The microemulsion domains in Figure 5 appear to increase in size as the segregation, χN_h, is reduced. To quantify this trend, we evaluate the two-point correlation function[36,45]

$$G(r) \equiv \langle \hat{\phi}_-(\mathbf{r}_0)\hat{\phi}_-(\mathbf{r}_0 + \mathbf{r}) \rangle = \frac{4\langle W_-(\mathbf{r}_0)W_-(\mathbf{r}_0 - \mathbf{r}) \rangle}{(\chi_b N_h)^2} - \frac{2\delta(\mathbf{r})}{\chi_b \rho_0} \tag{20}$$

which is plotted in Figure 9a for $\chi N_h = 2.31$. The average is obtained from $y-z$ slices through the middle of the BμE phase (see the inset). In addition to the ensemble average, we average over $\mathbf{r}_0$ and spherically average $\mathbf{r}$. In the lyotropic liquid crystal community, the correlation function is generally fit to the Teubner–Strey[46] form

$$G(r) = \frac{c}{r} e^{-r/\xi} \sin\left(\frac{2\pi r}{\lambda}\right) \tag{21}$$

to extract the characteristic size, λ, of the microemulsion domains. This functional form works well for $\chi N_h = 2.31$, as demonstrated in Figure 9a, but less so as the tricritical point is approached. Therefore, we simply define λ as two times the first zero of $G(r)$, which is plotted in Figure 9b as a function of χN_h.

Figure 10 compares the copolymer content, $\bar{\phi}_c$, in the coexisting phases extracted from the copolymer profile plotted in Figure 6b to the previous results from ref 32 obtained from plots like that of Figure 2. Our new results are more accurate. In the grand-canonical simulations, one needs to estimate the chemical potential where the system switches phases, whereas in the canonical simulations, the volumes of the three phases automatically adjust until the concentrations reach their equilibrium values. Furthermore, the new FTS use substantially larger simulation boxes and are thus less prone to finite-size effects. Indeed, it appears that the earlier results were affected. Although the binodals from ref 32 are in reasonable agreement at $\chi N_h = 2.31$, they become less so as χN_h is reduced. In particular,

https://dx.doi.org/10.1021/acs.macromol.0c02668
Macromolecules 2021, 54, 1329−1337

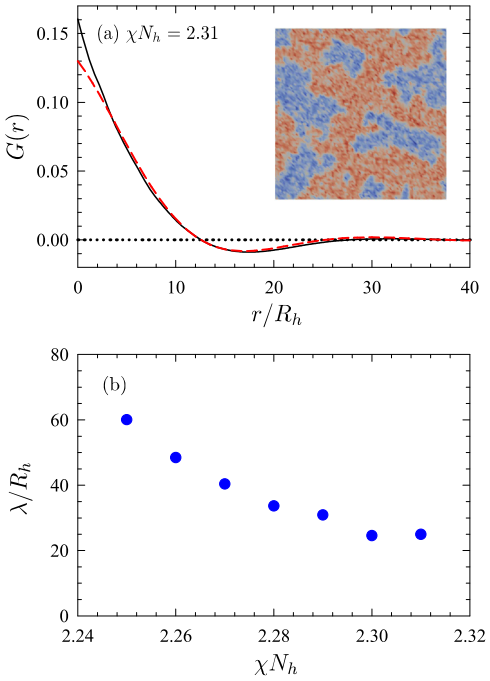

Figure 9. (a) Correlation function for the BμE phase at $\chi N_h = 2.31$, obtained from $72R_h \times 72R_h$ slices through the middle of the BμE phase (see the inset). The dashed curve shows a fit to the Teubner−Strey form in eq 21. (b) Characteristic domain size of the BμE phase.

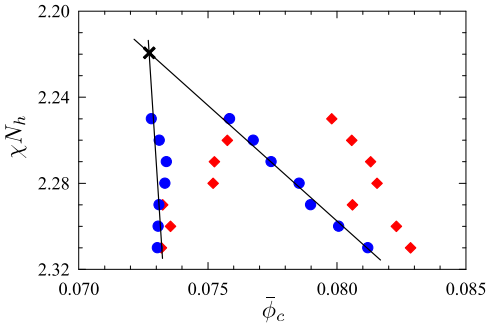

Figure 10. Binodals of the A + B + BμE region obtained from $\langle \phi_c(x) \rangle$ profiles (circles) compared to those of ref 32 (diamonds). Linear extrapolations estimate the position of the tricritical point (cross).

the three-phase window shifts to higher $\bar{\phi}_c$, as was the case in Figure 2 when the box size was too small. This is undoubtedly caused by the increasing size of the microemulsion domains plotted in Figure 9b.

The binodals should converge linearly as the tricritical point is approached.[47] Using this fact, we estimate the coordinates of the tricritical point to be $\bar{\phi}_c = 0.0727$ and $\chi N_h = 2.22$, based on the linear extrapolations in Figure 10. Interestingly, the position agrees well with that of the mean-field Lifshitz point, $\bar{\phi}_c = 2\alpha^2/(1 + 2\alpha^2) = 0.0741$ and $\chi N_h = 2(1 + 2\alpha^2) = 2.16$.[24] Figure 11 updates the phase diagram from ref 32 with our more accurate estimates of the A + B + BμE region and tricritical point. The remaining boundaries of the three-phase regions from the earlier simulations have significant error bars due to the uncertainty in determining the chemical potential of coexistence, as discussed above. Although the DIS and LAM phase must be separated by two-phase coexistence, as depicted in the schematic phase diagram of Figure 1b, the region was too narrow to resolve.

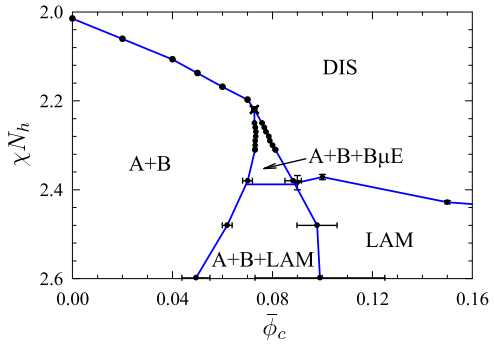

Figure 11. Phase diagram from ref 32 updated with our more accurate binodals of the A + B + BμE region.

DISCUSSION

Field-theoretic simulations have advanced considerably since the first application to ternary blends by Düchs et al.[21,22] nearly 2 decades ago. Those early studies were restricted to two-dimensional (2D) simulation boxes with 48 × 48 grid points. Even still, they struggled to cope with the large domains and slow dynamics of the microemulsion. In contrast, our simulations of A + B + BμE coexistence are performed on three-dimensional (3D) grids with 288 × 96 × 96 points, an increase of more than 3 orders of magnitude. Furthermore, the statistics are sufficient to map out the entire phase diagram. There are many advances that have contributed to this. Naturally, computers have improved, and in particular the advent of GPUs has been instrumental in scaling up the system size.[48] Improvements in the numerics[37] and algorithms[39] have also helped. Another important advance has been the switch from Monte Carlo to Langevin dynamics.[40] FTS have now evolved to the point where they are able to tackle problems that are beyond the capabilities of conventional particle-based simulations, and there will undoubtedly be further improvements to come.

Not only do our simulations strengthen the evidence for A + B + BμE coexistence in Figure 1b, they also seriously contradict the proposed microemulsion channel in Figure 1a, which implies that the A + B region is bounded by a second-order phase transition extending toward $T = 0$. If this was true, our histograms of the composition, $P(\bar{\phi}_-)$, would acquire a universal shape at the phase transition, independent of the system size.[33,49] In particular, $P(\bar{\phi}_-)$ would exhibit a local minimum at $\bar{\phi}_- = 0$ separating two symmetric peaks of approximate height 2.7 $P(0)$. However, the homopolymer-rich peak in Figure 3 remains far too narrow and the microemulsion peak at $\bar{\phi}_- = 0$ in Figure 4 shows no sign of disappearing. It is inconceivable that $P(\bar{\phi}_-)$ could possibly evolve into the universal shape at some intermediate value of μ.

The finite-size analyses in Figures 2−4 illustrate that simulation boxes of $L = 36R_h$ are sufficient for $\chi N_h = 2.31$. The smaller size of $L = 18R_h$ is almost fine but it causes a slight shift in the transition to higher μ, which then pushes the three-phase window to higher $\bar{\phi}_c$. This effect is also evident in Figure 10, where the results from ref 32 are shifted relative to our more accurate results obtained using larger boxes. The shift increases as the tricritical point is approached, presumably because of the increasing size of the microemulsion domains, λ. It is reasonable to assume that the box size must increase proportionally to λ to avoid finite-size effects. Given our tests at $\chi N_h = 2.31$, the boxes used for the three-phase coexistence in Figure 5 should be able

https://dx.doi.org/10.1021/acs.macromol.0c02668
Macromolecules 2021, 54, 1329−1337

to handle a doubling of λ. It was based on this criterion that we limited our simulations to $\chi N_h \gtrsim 2.25$.

Although our calculations could not be extended all the way to the tricritical point, they come close enough that we can extrapolate. As expected, the interfacial tensions in Figure 8 approach zero. The interfacial widths in Figure 7 increase but undoubtedly remain finite. On the other hand, it is difficult to tell from Figure 9b if the microemulsion domains remain finite or diverge prior to the tricritical point. Given the close proximity of the tricritical point to the mean-field Lifshitz point, we suspect that λ may indeed diverge, implying that the BμE transforms into a structureless disordered phase.

Xie et al.[19] have observed evidence of macrophase separation, but there has yet to be any clear experimental demonstration of the A + B + BμE coexistence. In water−oil−surfactant systems, however, three-phase coexistence is readily observed. This is certainly helped by the faster dynamics of the smaller molecules, but it is also aided by the density mismatch between water and oil. As a consequence, oil rises to the top and water sinks to the bottom of a container with the microemulsion sandwiched in between.[1,2] It may be possible to observe the same in a polymeric system, if, for example, component B is significantly denser than component A. A significant contrast in density would likely be accompanied by a strong χ parameter, and so low molecular weights would be required to access the ODT. Nevertheless, this would also help speed up the dynamics, and if necessary, the effect could be amplified by using a centrifuge.

If the interfacial tension between homopolymer and microemulsion, $\gamma_{B\mu E}$, is less than half the interfacial tension between the two homopolymers, $\gamma_{AB}/2$, then the microemulsion will wet the A/B interface forming a uniform layer, as illustrated in Figure 12a. However, if $\gamma_{B\mu E} > \gamma_{AB}/2$, then the wetting will be

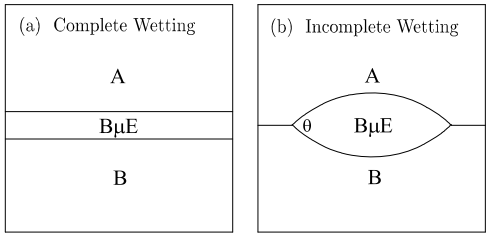

Figure 12. (a) Complete and (b) incomplete wetting of the A/B interface by BμE, in a system where component B is denser than component A. The contact angle, θ, is given by eq 22.

incomplete and the microemulsion will form a lens-shaped droplet with a contact angle of

$$\theta = 2\cos^{-1}\left(\frac{\gamma_{AB}}{2\gamma_{B\mu E}}\right) \tag{22}$$

as illustrated in Figure 12b. Incomplete wetting generally occurs in the case of conventional microemulsions.[50] Although our statistical noise is too large to say with certainty, the interfacial tensions plotted in Figure 8 indicate that the same will be true of polymeric microemulsions.

In the future, it would be interesting to delineate the microemulsion region within the DIS phase. There is no true phase transition separating microemulsion from simple disordered blends, and so the boundary has to be determined based on some appropriate property of a microemulsion. In the field of lyotropic liquid crystals, researchers regard the key characteristics of a microemulsion to be a correlation function $G(r)$ with a finite periodicity, λ, and a structure function, $S(k)$, with a peak at nonzero wavevector, k^*. As such, the two typical boundaries are the disorder line, defined as where $\lambda \to \infty$, and the Lifshitz line, defined as where $k^* \to 0$.[50] However, Düchs and Schmid[22] found these criteria to be unsatisfactory for the polymeric system, and so they instead developed an alternative criterion based on the curvature of the A/B interfaces relative to the domain size. It appeared to work well for their 2D simulations, but it has yet to be applied to 3D simulations.

Another important issue that could be addressed is the effect on three-phase coexistence due to asymmetries in the diblock composition, the size of the homopolymers, and the statistical segment lengths.[13] The practicality of determining the three-phase region from plots like that of Figure 2 calculated with grand-canonical simulations relies on perfect symmetry, whereby the coexistence occurs at equal homopolymer chemical potentials. However, there is no such necessity for plots like that of Figure 6 calculated with the canonical simulations. It would also be useful to consider polydispersity, which is expected to increase the size of the A + B + BμE region at the expense of A + B + LAM coexistence.[51]

SUMMARY

Our new field-theoretic simulations provide strong evidence that ternary blends of A-homopolymer, B-homopolymer, and AB diblock produce an equilibrium A + B + BμE coexistence region that terminates in a tricritical point at high temperature as depicted in Figure 1b as opposed to the microemulsion channel depicted in Figure 1a. First, the consistency among different system sizes in Figure 2 illustrates that the sudden jump in copolymer concentration, $\langle\bar{\phi}_c\rangle$, with increasing chemical potential, μ, is the result of a first-order phase transition corresponding to three-phase coexistence. Second, the histograms in Figures 3 and 4 further confirm that the results are free of significant finite-size effects. Third, the histograms contradict the implication of Figure 1a that the A + B region is entirely bounded by a second-order phase transition.

The direct simulations of A + B + BμE coexistence in Figure 5 cement this conclusion. Furthermore, these are the first simulations for the interfaces of a microemulsion, certainly for polymeric systems and, as far as we are aware, also for conventional water−oil−surfactant mixtures. From these simulations, we were able to evaluate the widths, $w_{B\mu E}$ and w_{AB}, and tensions, $\gamma_{B\mu E}$ and γ_{AB}, of the homopolymer/microemulsion and homopolymer/homopolymer interfaces, respectively. As the tricritical point is approached, the interfacial widths increase but remain finite and the interfacial tensions approach zero.

The simulations of A + B + BμE coexistence also provided more accurate phase boundaries, first because of the larger system sizes and second because the coexisting phases are able to freely adjust their copolymer content, $\bar{\phi}_c$. The extrapolation of these boundaries also provides a more accurate estimation of the tricritical point, which turns out to coincide closely with the position of the mean-field Lifshitz point. This is consistent with our observation that the domain size of the BμE appears to diverge as the tricritical point is approached, implying that it reduces to a structureless disordered phase.

Hopefully, this study will motivate an experimental search for A + B + BμE coexistence. We propose using a system where the mass densities of the A and B components are sufficiently different that the heavier and lighter homopolymer-rich phases

https://dx.doi.org/10.1021/acs.macromol.0c02668
Macromolecules 2021, 54, 1329−1337

segregate to the bottom and top of the container, respectively, with the microemulsion phase in between. It would then be interesting to observe if the BμE wets the A/B interface. Our simulations suggest that $\gamma_{AB} < 2\gamma_{B\mu E}$, which would result in incomplete wetting as is the case for conventional lyotropics.

■ ASSOCIATED CONTENT

Supporting Information

The Supporting Information is available free of charge at https://pubs.acs.org/doi/10.1021/acs.macromol.0c02668.

Video showing the evolution of the morphology in Figure 5c as a function of τ during the simulation (MP4)

■ AUTHOR INFORMATION

Corresponding Authors

Russell K. W. Spencer − *Department of Chemical Engineering, Department of Physics & Astronomy, and Waterloo Institute for Nanotechnology, University of Waterloo, Waterloo, Ontario N2L 3G1, Canada;* orcid.org/0000-0002-4814-9010; Email: r6spence@uwaterloo.ca

Mark W. Matsen − *Department of Chemical Engineering, Department of Physics & Astronomy, and Waterloo Institute for Nanotechnology, University of Waterloo, Waterloo, Ontario N2L 3G1, Canada;* orcid.org/0000-0003-2099-0892; Email: mwmatsen@uwaterloo.ca

Complete contact information is available at: https://pubs.acs.org/10.1021/acs.macromol.0c02668

Notes

The authors declare no competing financial interest.

■ ACKNOWLEDGMENTS

We thank Marcus Müller for stimulating discussions and for encouraging us to perform the finite-size analysis. Computer resources were provided by Compute Canada.

■ REFERENCES

(1) Prévost, S.; Gradzielski, M.; Zemb, T. Self-assembly, phase behaviour and structural behaviour as observed by scattering for classical and non-classical microemulsions. *Adv. Colloid Interface Sci.* **2017**, *247*, 374−396.

(2) Tartaro, G.; Mateos, H.; Schirone, D.; Angelico, R.; Palazzo, G. Microemulsion Microstructure(s): A Tutorial Review. *Nanomatertials* **2020**, *10*, No. 1657.

(3) Salager, J.-L.; Forgiarini, A. M.; Márquez, L.; Manchego, L.; Bullón, J. How to Attain an Ultralow Interfacial Tension and a Three-Phase Behavior with a Surfactant Formulation for Enhanced Oil Recovery: A Review. Part 2. Performance Improvement Trends from Winsor's Premise to Currently Proposed Inter- and Intra-Molecular Mixtures. *J. Surfactants Deterg.* **2013**, *16*, 631−663.

(4) Bates, F. S.; Maurer, W. W.; Lipic, P. M.; Hillmyer, M. A.; Almdal, K.; Mortensen, K.; Fredrickson, G. H.; Lodge, T. P. Polymeric Bicontinuous Microemulsions. *Phys. Rev. Lett.* **1997**, *79*, 849−852.

(5) Hillmyer, M. A.; Maurer, W. W.; Lodge, T. P.; Bates, F. S.; Almdal, K. Model bicontinuous microemulsions in ternary homopolymer block copolymer blends. *J. Phys. Chem. B* **1999**, *103*, 4814−4824.

(6) Schwahn, D.; Mortensen, K.; Frielinghaus, H.; Almdal, K. Crossover from 3D ising to isotropic Lifshitz critical behavior in a mixture of a homopolymer blend and diblock copolymer. *Phys. Rev. Lett.* **1999**, *82*, 5056−5059.

(7) Schwahn, D.; Mortensen, K.; Frielinghaus, H.; Almdal, K.; Kielhorn, L. Thermal composition fluctuations near the isotropic Lifshitz critical point in a ternary mixture of a homopolymer blend and diblock copolymer. *J. Chem. Phys.* **2000**, *112*, 5454−5472.

(8) Krishnan, K.; Almdal, K.; Burghardt, W. R.; Lodge, T. P.; Bates, F. S. Shear-induced nano-macro structural transition in a polymeric bicontinuous microemulsion. *Phys. Rev. Lett.* **2001**, *87*, No. 098301.

(9) Pipich, V.; Schwahn, D.; Willner, L. Ginzburg Number of a Homopolymer−Diblock Copolymer Mixture Covering the 3D-Ising, Isotropic Lifshitz, and Brasovskii Classes of Critical Universality. *Phys. Rev. Lett.* **2005**, *94*, No. 117801.

(10) Habersberger, B. M.; Gillard, T. M.; Hickey, R. J.; Lodge, T. P.; Bates, F. S. Fluctuation Effects in Symmetric Diblock Copolymer−Homopolymer Ternary Mixtures near the Lamellar−Disorder Transition. *ACS Macro Lett.* **2014**, *3*, 1041−1045.

(11) Walker, C. N.; Bryson, K. C.; Hayward, R. C.; Tew, G. N. Wide Bicontinuous Compositional Windows from Co-Networks Made with Telechelic Macromonomers. *ACS Nano* **2014**, *8*, 12376−12385.

(12) Hickey, R. J.; Gillard, T. M.; Irwin, M. T.; Lodge, T. P.; Bates, F. S. Structure, viscoelasticity, and interfacial dynamics of a model polymeric bicontinuous microemulsion. *Soft Matter* **2016**, *12*, 53.

(13) Hickey, R. J.; Gillard, T. M.; Irwin, M. T.; Morse, D. C.; Lodge, T. P.; Bates, F. S. Phase Behavior of Diblock Copolymer−Homopolymer Ternary Blends: Congruent First-Order Lamellar−Disorder Transition. *Macromolecules* **2016**, *49*, 7928−7944.

(14) Lee, J. H.; Ruegg, M. L.; Balsara, N. P.; Zhu, Y.; Gido, S. P.; Krishnamoorti, R.; Kim, M.-H. Phase Behavior of Highly Immiscible Polymer Blends Stabilized by a Balanced Block Copolymer Surfactant. *Macromolecules* **2003**, *36*, 6537−6548.

(15) Jones, B. H.; Lodge, T. P. Hierarchically Structured Materials from Block Polymer Confinement within Bicontinuous Microemulsion-Derived Nanoporous Polyethylene. *ACS Nano* **2011**, *5*, 8914−8927.

(16) Kipp, D.; Wodo, O.; Ganapathysubramanian, B.; Ganesan, V. Achieving Bicontinuous Microemulsion Like Morphologies in Organic Photovoltaics. *ACS Macro Lett.* **2015**, *4*, 266−270.

(17) Kipp, D.; Mok, J.; Strzalka, J.; Darling, S. B.; Ganesan, V.; Verduzco, R. Rational Design of Thermally Stable, Bicontinuous Donor/Acceptor Morphologies with Conjugated Block Copolymer Additives. *ACS Macro Lett.* **2015**, *4*, 867−871.

(18) Shim, J.; Bates, F. S.; Lodge, T. P. Bicontinuous Microemulsions in Partially Charged Ternary Polymer Blends. *ACS Macro Lett.* **2019**, *8*, 1166−1171.

(19) Xie, S.; Meyer, D. J.; Wang, E.; Bates, F. S.; Lodge, T. P. Structure and Properties of Bicontinuous Microemulsions from Salt-Doped Ternary Polymer Blends. *Macromolecules* **2019**, *52*, 9693−9702.

(20) Matsen, M. W. Field theoretic approach for block polymer melts: SCFT and FTS. *J. Chem. Phys.* **2020**, *152*, No. 110901.

(21) Düchs, D.; Ganesan, V.; Fredrickson, G. H.; Schmid, F. Fluctuation Effects in Ternary AB + A + B Polymeric Emulsions. *Macromolecules* **2003**, *36*, 9237−9248.

(22) Düchs, D.; Schmid, F. Formation and structure of the microemulsion phase in two-dimensional ternary AB+A+B polymeric emulsions. *J. Chem. Phys.* **2004**, *121*, 2798−2805.

(23) Yadav, M.; Bates, F. S.; Morse, D. C. Effects of Segment Length Asymmetry in Ternary Diblock Copolymer-Homopolymer Mixtures. *Macromolecules* **2019**, *52*, 4091−4102.

(24) Broseta, D.; Fredrickson, G. H. Phase equilibria in copolymer/homopolymer ternary blends: Molecular weight effect. *J. Chem. Phys.* **1990**, *93*, 2927−2938.

(25) Fredrickson, G. H.; Helfand, E. Fluctuation effects in the theory of microphase separation in block 'copolymers. *J. Chem. Phys.* **1987**, *87*, 697−705.

(26) Grzywacz, P.; J. Qin, J.; Morse, D. C. Renormalization of the one-loop theory of fluctuations in polymer blends and diblock copolymer melt. *Phys. Rev. E* **2007**, *76*, No. 061802.

(27) Kielhorn, L.; Muthukumar, M. Fluctuation theory of diblock copolymer/homopolymer blends and its effects on the Lifshitz point. *J. Chem. Phys.* **1997**, *107*, 5588−5608.

(28) Pram, A.; Stell, G. Isotropic Lifshitz point in $2 < d < 4$ dimensions. *Phys. Rev. B* **1977**, *16*, 4146−4153.

(29) Hornreich, R. M.; Liebmann, R.; Schuster, H. G.; Selke, W. Lifshitz Points in Ising Systems. *Z. Phys. B: Condens. Matter Quanta* **1979**, *35*, 91−97.
(30) Kudlay, A.; Stepanow, S. On the behavior of the Lifshitz line in ternary homopolymer/diblock copolymer blends. *Macromol. Theory Simul.* **2002**, *11*, 16−21.
(31) Zappalà, D. Isotropic Lifshitz point in the O(N) theory. *Phys. Lett. B* **2017**, *773*, 213−218.
(32) Vorselaars, B.; Spencer, R. K. W.; Matsen, M. W. Instability of the microemulsion channel in block copolymer-homopolymer blends. *Phys. Rev. Lett.* **2020**, *125*, No. 117801.
(33) Müller, M.; Schick, M. Bulk and interfacial thermodynamics of a symmetric, ternary homopolymer-copolymer mixture: A Monte Carlo study. *J. Chem. Phys.* **1996**, *105*, 8885−8901.
(34) Thompson, R. B.; Matsen, M. W. Effective interactions between monolayers of block copolymer compatibilzer in a polymer blends. *J. Chem. Phys.* **2000**, *112*, 6863−6872.
(35) Fredrickson, G. H.; Ganesan, V.; Drolet, F. Field-Theoretic Computer Simulation Methods for Polymers and Complex Fluids. *Macromolecules* **2002**, *35*, 16−39.
(36) Muller, M.; Schmid, F. *Advanced Computer Simulation Approaches for Soft Matter Sciences II*; Holm, C.; Binder, K., Eds.; Springer-Verlag: Berlin, Germany, 2005.
(37) Stasiak, P.; Matsen, M. W. Efficiency of pseudo-spectral algorithms with Anderson mixing for the SCFT of periodic block-copolymer phases. *Eur. Phys. J. E* **2011**, *34*, No. 110.
(38) Ranjan, A.; Qin, J.; Morse, D. C. Linear Response and Stability of Ordered Phases of Block Copolymer Melts. *Macromolecules* **2008**, *41*, 942−954.
(39) Spencer, R. K. W.; Matsen, M. W. Fluctuation effects in blends of A+B homopolymers with AB diblock copolymer. *J. Chem. Phys.* **2018**, *148*, No. 204907.
(40) Beardsley, T. M.; Spencer, R. K. W.; Matsen, M. W. Computationally efficient field-theoretic simulations for block copolymer melts. *Macromolecules* **2019**, *52*, 8840−8848.
(41) Düchs, D.; Delaney, K. T.; Fredrickson, G. H. A multi-species exchange model for fully fluctuating polymer field theory simulations. *J. Chem. Phys.* **2014**, *141*, No. 174103.
(42) Olvera de la Cruz, M.; Edwards, S. F.; Sanchez, I. C. Concentration Fluctuations in Polymer Blend Thermodynamics. *J. Chem. Phys.* **1988**, *89*, 1704−1708.
(43) Stasiak, P.; Matsen, M. W. Monte Carlo field-theoretic simulations for melts of symmetric diblock copolymer. *Macromolecules* **2013**, *46*, 8037−8045.
(44) Riggleman, R. A.; Fredrickson, G. H. Field-theoretic simulations in the Gibbs ensemble. *J. Chem. Phys.* **2010**, *132*, No. 024104.
(45) Spencer, R. K. W.; Matsen, M. W. Critical point of symmetric binary homopolymer blends. *Macromolecules* **2016**, *49*, 6116−6125.
(46) Teubner, M.; Strey, R. Origin of the Scattering Peak in Microemulsions. *J. Chem. Phys.* **1987**, *87*, 3195−3200.
(47) Jain, A. K.; Landau, D. P. Monte Carlo Study of the FCC Blume-Capel Model. *Phys. Rev. B* **1980**, *22*, 445−452.
(48) Cheong, G. K.; Chawla, A.; Morse, D. C.; Dorfman, K. D. Open-source code for self-consistent field theory calculations of block polymer phase behavior on graphics processing units. *Eur. Phys. J. E* **2020**, *43*, No. 15.
(49) Hilfer, R.; Wilding, N. B. Are critical finite-size scaling functions calculable from knowledge of an appropriate critical exponent. *J. Phys. A: Math. Gen.* **1995**, *28*, L281−L286.
(50) Schubert, K.-V.; Strey, R. Small-angle neutron scattering from microemulsions near the disorder line in water/formamide−octane-C_iE_j systems. *J. Chem. Phys.* **1991**, *95*, 8532−8545.
(51) Thompson, R. B.; Matsen, M. W. Improving polymeric microemulsions with block copolymer polydispersity. *Phys. Rev. Lett.* **2000**, *85*, 670−673.

https://dx.doi.org/10.1021/acs.macromol.0c02668
Macromolecules 2021, 54, 1329−1337